

Effects of all-atom force fields on amyloid oligomerization: Replica exchange molecular dynamics simulations of the A β _{16–22} dimer and trimer

Phuong H. Nguyen^{1,3*}, Mai Suan Li², Philippe Derreumaux^{3†}

¹*Institute of Physical and Theoretical Chemistry, Goethe University,
Max-von-Laue-Str. 7, D-60438 Frankfurt, Germany*

²*Institute of Physics, Polish Academy of Sciences,
Al. Lotnikow 32/46, 02-668 Warsaw, Poland*

³*Laboratoire de Biochimie Théorique,
UPR 9080 CNRS, IBPC, Université Paris 7
13 rue Pierre et Marie Curie, 75005, Paris, France
and Institut Universitaire de France*

(Dated: March 15, 2011)

Abstract

The aim of this work is to investigate the effects of molecular mechanics force fields on amyloid peptide assembly. To this end, we performed extensive replica exchange molecular dynamics (REMD) simulations on the monomer, dimer and trimer of the seven-residue fragment of the Alzheimer’s amyloid- β peptide, A β _{16–22}, using the AMBER99, GROMOS96 and OPLS force fields. We compared the force fields by analysing the resulting global and local structures as well as the free energy landscapes at 300 K. We show that AMBER99 strongly favors helical structures for the monomer and does not predict any β -sheet structure for the dimer and trimer. In contrast, the dimer and trimer modeled by GROMOS96 form antiparallel β -sheet structures, while OPLS predicts diverse structures. Overall, the free energy landscapes obtained by three force fields are very different, and we also note a weak structural dependence of our results on temperature. The implications of this computational study on amyloid oligomerization, fibril growth and inhibition are also discussed.

* Email: phuong.nguyen@ibpc.fr

† Email: philippe.derreumaux@ibpc.fr

I. INTRODUCTION

A large body of experimental data suggests that oligomeric intermediates are the primary causes of several human neurodegenerative diseases, such as Alzheimer and Parkinson, and other pathologies such as type II diabetes [1–5]. These findings have motivated intensive study of the structure and assembly dynamics of the early and late steps of amyloids. Considerable insight has been provided by various experimental techniques, including TEM, AFM, X-ray fiber diffraction [6–8], solid-state NMR [9–11], x-ray crystallography [12] and infrared (IR) spectroscopy [13, 14]. These studies have confirmed that prefibrillar oligomers are very unstable with diverse morphologies sampled and undergo rapid conformational fluctuations. In contrast, amyloid fibrils adopt a cross- β structure with the β -sheets perpendicular to the fibril axis, and a hydrogen bond network parallel to the fibril axis [15]. These experiments also showed that fibril formation is governed by multiple factors such as the hydrophobicity of side chains [16] and notably aromatic interactions [17], the net charge and secondary structure propensity [18–20] and the pattern of polar and non-polar residues [21].

First-principles theoretical study of amyloid peptide aggregation represents a considerable challenge. It requires an efficient sampling of conformational space that can be obtained with enhanced conformational search techniques, and an accurate potential energy function or force field (ff). Several protein coarse-grained lattice [22–26] and off-lattice models [27–33], and all-atom force fields [34–39] have been employed. Although these computational studies provided valuable insights into protofibril stability and growth, the early steps of oligomerization, the role of the population of the fibril-prone conformation, and of the secondary structure content of the monomer on the self-assembly kinetics [25, 28, 40–43], the lack of experimental data on the transient oligomers makes it difficult to validate these theoretical results and one may ask how these results depend on the force field.

The influence of the GROMOS [44], OPLS/AA [45], CHARMM [46], and AMBER ff94, ff99, ff99SB, ff03 force fields [47–49] on the equilibrium structures of non-amyloid peptides has already reported. Results on dipeptides [50], tripeptides [51], α -helical peptides [36, 52–55], two β -hairpins and Trp-cage [54] have shown that AMBER99 ff favors helical structures over extended β -strand conformations, GROMOS96 ff may overestimate β conformations, while OPLS ff generates a better balance between α and extended (β and polyproline II,

PPII) structures.

The A β peptide of the Alzheimer’s disease and one long truncated variant have also been discussed in their monomeric forms using various force fields. Using REMD simulations with 52 replicas from 270 to 600 K, each for 225 ns coupled to AMBER ff99SB and the TIP4P-Ew water model, Sgourakis et al. calculated the J-coupling constants, $^3J_{HNH\alpha}$, of A β_{1-42} and obtained a Pearson correlation coefficient (PCC) of 0.52 with NMR experiment [56]. This PCC value is similar to the one obtained previously for the same system using OPLS/AA and TIP3P water model (60ns/replica and PCC of 0.48) and differs strikingly from the PCC value of -0.01 using GROMOS96 [57]. The A β_{15-35} peptide has also been studied by Langevin dynamics simulations using CHARMM, OPLS/AA and GS-AMBER94, but there is no proof that convergence of the simulations was reached [58]. Overall, a systematic comparison of classical all-atom force fields on the structures and energetics of amyloid oligomers has not been carried out.

Ideally, we would like to consider the dimer and trimer of the A β_{1-40} or A β_{1-42} peptides as they are the proximate neurotoxic species in Alzheimer’s disease [59]. Such a structural characterization is, however, out of reach using all-atom models in explicit solvent due to the slow convergence of simulations to equilibrium and one resorts to coarse-grained protein models with implicit solvent [42, 60] or short A β fragments that form amyloid fibrils by themselves [58, 61, 62]. It is to be noted that although these shorter fragments may not be fully representative of the whole A β peptide, they help explore fundamental aspects of the thermodynamics and kinetics of amyloid aggregation [43, 63].

As a first step toward determining force field effects on the early formed amyloid oligomers, we study the monomer, dimer, and trimer formed by the seven-residue fragment A β_{16-22} using the AMBER99 [48], GROMOS96 [44] and OPLS/AA [45] force fields. The ability of this peptide to form fibrils in vitro with antiparallel ordering of the β -strands was ascertained by experiments [64]. Low molecular weight aggregates of A β_{16-22} were also studied by various computational studies using either all-atom representation but limited sampling of configuration space [35, 65, 66] or more extensive simulations with simplified protein models [33, 36, 67–69].

Providing A β_{16-22} monomer to trimer results using all-atom models which have been devised to study biomolecular systems is beyond the scope of our work for two reasons. Firstly, the present MD and REMD results on the A β_{16-22} monomer to trimer using three

force fields already require 90 days for the monomer (using 1 core), 70 days for the dimer (using 32 cores) and 80 days for the trimer (using 40 cores). Secondly, existing classical force fields are permanently subject to improvement, but their successful applications to many systems remain to be validated. For instance, the CHARMM22 force field with CMAP correction, not discussed here and designed to make α -helices more stable, failed in folding simulations of a WW protein domain [70]. Similarly, the AMBER99SB ff [49] yielded improved agreements between calculated and NMR/crystallographic side-chain torsion distributions, but failed for alanine-based peptides [71]. The recently designed AMBER ff03* [71] provided a meaningful sampling of a α -helix and β -sheet peptides [72], but discrepancies were observed between conformational distributions of a polyalanine peptide in solution obtained from molecular dynamics force fields and amide I' band profiles [73]. Finally, the AMBER99SB ILDN ff was found to work well on the three model peptides, but Shaw et al. clearly stated that its success does not guarantee it is a suitable ff for all sequences [74].

Overall, our simulations show that the GROMOS96 and AMBER99 force fields are biased toward amyloid-like and α -helical structures, respectively. In contrast, the OPLS force field provides a wide conformational distribution. The implications of our results on amyloid oligomerization, fibril growth and inhibition are discussed.

II. MATERIAL AND METHODS

A. Force fields

Most force fields for biomolecular simulations are represented by an empirical potential-energy expression of the form

$$\begin{aligned}
 V = & \sum_{\text{bonds}} K_r (r - r_{\text{eq}})^2 + \sum_{\text{angles}} K_\theta (\theta - \theta_{\text{eq}})^2 \\
 & + \sum_{\text{dihedrals}} \frac{V_n}{2} [1 + \cos(n\phi - \delta_n)] + \sum_{i < j} \left[\frac{A_{ij}}{R_{ij}^{12}} - \frac{B_{ij}}{R_{ij}^6} + \frac{q_i q_j}{\epsilon R_{ij}} \right]. \quad (1)
 \end{aligned}$$

Here, the first three terms describe the short-range interactions, where the bonds and angles are represented by a simple harmonic expression and neglect the changes in distance between the first and third atom associated with a bond angle [75, 76] and the dihedral

energies are modeled by a Fourier expansion. The last sum accounts for the intermolecular or nonbonded interactions, where the van der Waals interaction is treated by a 6 – 12 potential and the electrostatic interactions are modeled by a Coulomb potential of atom-centered point charges. For a discussion on the various force-field parametrization procedures and development, see, for example, Refs. [44–47]. In this work, we have employed three force fields: parm99.dat version of AMBER [48], 43A1 version of GROMOS [44] and the all-atom version of the OPLS force field [45]. For simplicity, throughout the paper we referred to as $A\beta_1$, $A\beta_2$ and $A\beta_3$ for the monomer, dimer and trimer of $A\beta_{16-22}$, respectively.

B. Simulation details

The simulated sequence is Lys-Leu-Val-Phe-Phe-Ala-Glu, i.e. free of Ace and NH2 capped ends. We use the SPC (Simple Point Charge) [77] water model with the GROMOS force field, and the TIP3P water model [78] with the AMBER and OPLS force fields. The initial configuration of the $A\beta_1$ was extracted from the structure of the $A\beta_{10-35}$ peptide available in the Protein Data Bank (ID: 1hz3) [79]. The initial configurations of the $A\beta_2$ and $A\beta_3$ were obtained by replicating the individual $A\beta_1$ structure in random orientations and the $A\beta_1$, $A\beta_2$ and $A\beta_3$ systems were placed in periodic octahedral boxes containing 1168, 3089 and 3306 water molecules, with concentrations of 46, 35 and 43 mM, respectively. The solvated systems were then minimized using the steepest descent method and were equilibrated for 1 ns at constant pressure (1 atm) and temperature ($T = 300$ K), respectively, using the Berendsen coupling method [80]. The systems were subsequently equilibrated at constant temperature ($T = 300$ K) and constant volume for 1 ns. The final structure was used as the starting structure for the $A\beta_1$ MD simulation and for all the replicas of the $A\beta_2$ and $A\beta_3$ systems.

The GROMACS program suite [81, 82] was employed for all simulations. The equations of motion were integrated by using a leap-frog algorithm with a time step of 2 fs. Covalent bond lengths were constrained via the SHAKE [83] procedure with a relative geometric tolerance of 10^{-4} . We used the particle-mesh Ewald method to treat the long-range electrostatic interactions [84]. The nonbonded interaction pair-list was updated every 5 fs, using a cutoff of 1.2 nm. The Berendsen coupling method [80] was used to couple each system to the heat bath with a relaxation time of 0.1 ps.

For MD simulation, the $A\beta_1$ system was run at 300 K and constant volume for 500 ns. For REMD simulations, given the lowest (290 K) and highest (400 K) temperatures and requesting an acceptance ratio of $\approx 20\%$, the temperatures of replicas were determined by using the method recently proposed by Patriksson and van der Spoel [85, 86]. This resulted in 32 and 40 replicas for the $A\beta_2$ and $A\beta_3$ systems, respectively. Exchanges between replicas were attempted every 1.5 ps, large enough compared to the coupling time of the heat bath. Each replica was run for 55 ns and the data were collected every 2 ps. The first 5 ns of all trajectories were excluded for analysis. Convergence of the simulations were assessed by block analysis.

C. Data analysis

To characterize the oligomers of $A\beta$, we used several quantities. Let \vec{u}_i be the unit vector linking N and C-termini of the i -th peptide. The nematic order parameter P_2 [66], is defined as follows

$$P_2 = \sum_{i=1}^N \frac{|\vec{r}_{NC}^i|}{L_i} P_2^0, \quad (2)$$

where $P_2^0 = \frac{1}{2N} \sum_{i=1}^N \frac{3}{2} (\vec{u}_i \cdot \vec{d})^2 - \frac{1}{2}$ with \vec{d} (the director) is a unit vector defining the preferred direction of alignment, N is the number of peptides, and \vec{r}_{NC}^i is the end-to-end vector that connects the C_α atom termini of the i -th peptide. The end-to-end distance in the fully stretched state $L_i = (N_i - 1)a$, where N_i is a number of amino acids in i -th monomer and a ($\approx 4 \text{ \AA}$) is the distance between two consecutive C_α atoms. We define that the system has the propensity to form fibril-like conformation if P_2 is > 0.5 [66].

To assess the relative alignment of the i -th peptide with respect to the j -th peptide, we calculated the product between two unit vectors $\vec{u}_i \cdot \vec{u}_j$. A negative (positive) value of this cosine content $c(ij)$ reflects a tendency for antiparallel (parallel) alignment.

Principal component analysis (PCA) is an efficient method to represent the conformational distribution of a $3N$ -dimensional system in terms of a few “principal” components [87–90]. In this work, we used the dihedral angle PCA (dPCA) [91] method, that uniquely defines the distance in the space of periodic dihedral angles using the variables $\mathbf{q} = \{q_k\}$ with $q_k = \cos(\alpha_k)$ and $q_{k+1} = \sin(\alpha_k)$. Here, $\alpha_k \in \{\phi_k, \psi_k\}$ and $k = 1 \dots 2Np - 1$, with N and p being the number of dihedral angles of a peptide and the number of peptides, respectively.

The correlated internal motions are probed using the covariance matrix

$$\sigma_{ij} = \langle (q_i - \langle q_i \rangle)(q_j - \langle q_j \rangle) \rangle, \quad (3)$$

where $\langle \dots \rangle$ denotes the average over all sampled conformations. By diagonalizing σ , we obtain $2Np$ eigenvectors $\mathbf{v}^{(i)} = \{v_{ni}\}$ (v_{ni} is the n -th component of the i -th eigenvector) and eigenvalues λ_n , which are rank-ordered in descending order, i.e., λ_1 represents the largest eigenvalue. The eigenvectors and eigenvalues of σ yield the modes of collective motion and their amplitudes. The i -th principal component is defined as $V_i = \mathbf{v}^{(i)} \cdot \mathbf{q}$. It has been shown that a large part of the system's fluctuations can be described in terms of only a first few principal components [87–90]. The free energy landscape spanned by n principal components $V = (V_1, \dots, V_n)$ is given by $G(V) = -k_B T [\ln P(V) - \ln P_{\max}]$, where $P(V)$ is the probability distribution obtained from a histogram of the MD data, P_{\max} is the maximum of the distribution, which is subtracted to ensure that $G = 0$ for the lowest free energy minimum. We used dPCA to compute the free energy landscapes using mainly the first two eigenvectors V_1 and V_2 .

We monitored the secondary structure composition of $A\beta_2$ and $A\beta_3$ systems using the STRIDE program [92], and of the $A\beta_1$ using the "broad" definition as reported in Ref. [35]. Following this definition, if (ϕ, ψ) angles are discretized into 20 intervals of 18° , then a β state corresponds to the vertices of the polygon $(-180, 180)$, $(-180, 126)$, $(-162, 126)$, $(-162, 108)$, $(-144, 108)$, $(-144, 90)$, $(-50, 90)$, $(-50, 180)$ on the Ramachandran plot, and the α helix state is confined to the polygon $(-90, 0)$, $(-90, -54)$, $(-72, -54)$, $(-72, -72)$, $(-36, -72)$, $(-36, -18)$, $(-54, -18)$, $(-54, 0)$, all other regions are considered as coil. The peptide is in the β (α helix) conformation if (i) the (ϕ, ψ) angles of any two consecutive residues are in the corresponding β (α helix) states, and (ii) no two consecutive residues are in α helix (β) states. If neither β nor α helix conformations are assigned, then the peptide is classified as random coil. For the monomer, and for comparison with previous simulations, we also defined the PPII conformation following the definition of Garcia [93]. A residue is in the PPII state if $-120^\circ \leq \phi \leq -30^\circ$ and $60^\circ \leq \psi \leq 180^\circ$, and the peptide is in the PPII conformation if three or more consecutive residues are in the PPII state.

Finally, we also calculated the number of inter-peptide and intra-peptide side-chain–side-chain contacts: N_c^{inter} and N_c^{intra} . A contact is formed if the distance between the centers of mass of two residues is less than 6.5 \AA .

III. RESULTS AND DISCUSSION

A. Global and local pictures at 300 K

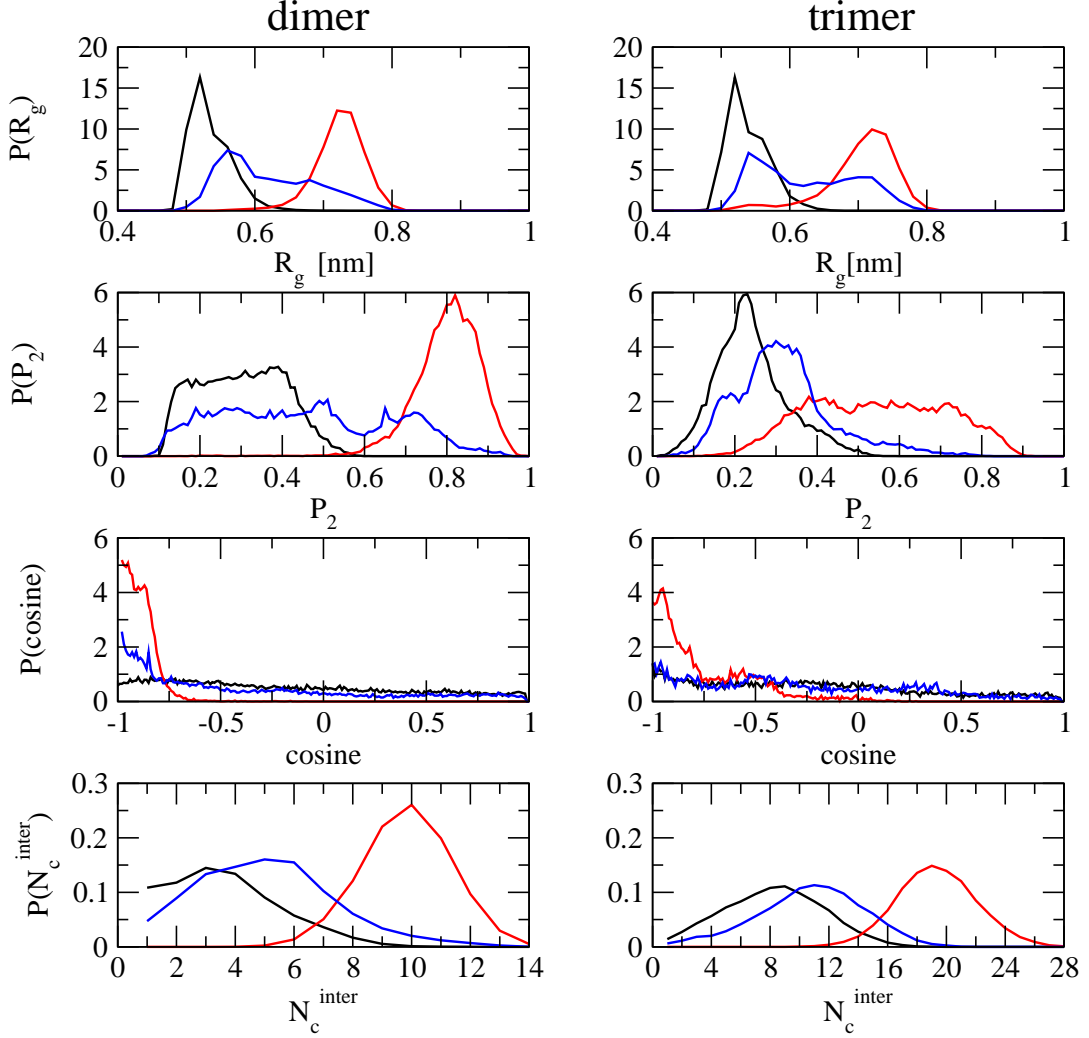


FIG. 1: Normalized distribution of the radius of gyration R_g , the order parameter P_2 , the cosine of the angle between the end-to-end vectors of two peptides referred to as $c(ij)$ for the dimer and the conditional probability for the trimer, and the total inter-peptide contacts N_c^{inter} . Shown are results obtained by AMBER (black), GROMOS (red) and OPLS (blue). Left panels and right panels show results for Aβ₂ and Aβ₃, respectively.

To obtain a global picture of Aβ₂ and Aβ₃ configurations, we calculated the averaged distribution $P(q) = \sum_p P(q_p)/p$, where q_p is a reaction coordinate of the p -th peptide. We considered four coordinates: the radius of gyration, the order parameter P_2 , the $c(ij)$ values,

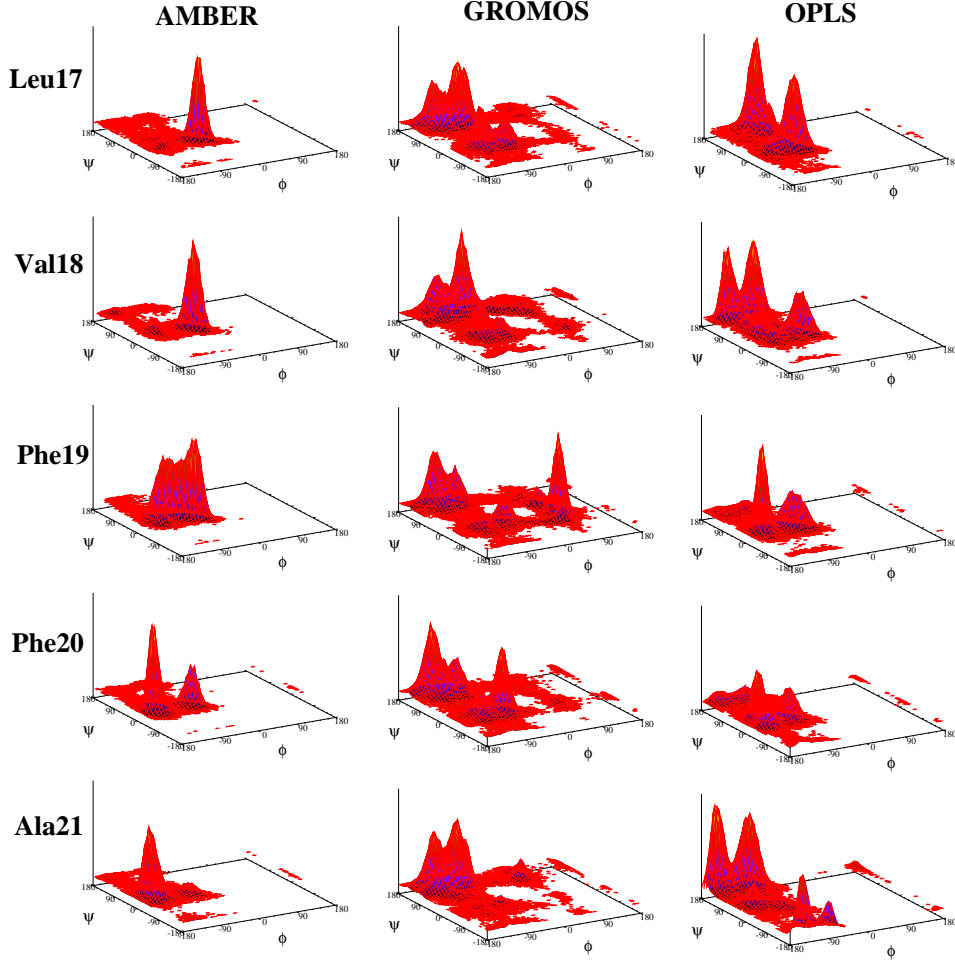


FIG. 2: Ramachandran ϕ, ψ probability distributions of the five inner residues of $A\beta_1$ in water as obtained from 500 ns MD simulations employing the three force fields.

and the total number of intermolecular contacts. Results are shown in Fig. 1.

The radius of gyration $R_g = (\sum_i m_i d_i^2)^{1/2} / (\sum_i m_i)^{1/2}$ is defined as the average of the mass-weighted squared distances of all atoms to the center of mass. As seen from Fig. 1, the R_g distributions for $A\beta_2$ and $A\beta_3$ are very similar. For each system, AMBER and GROMOS show a single-peak distribution. However, the structures are compact using AMBER ($R_g \approx 0.5$ nm), while they are extended using GROMOS ($R_g \approx 0.75$ nm). OPLS, on the other hand, displays a broad R_g distribution. If we consider the value of $R_g = 0.62$ nm as the threshold between compact and extended structures, OPLS results in 60 % and 40 % of compact and extended structures, respectively.

The order parameter P_2 depends not only on the relative orientational order, but also on

the end-to-end distances of the peptides. Here, the distance is measured between the C α carbon atoms of Lys16 and Glu22. A β_2 with AMBER has a very small $P_2 \approx 0.3$. With GROMOS, A β_2 is extremely ordered as indicated by a P_2 value of ≈ 1 , while OPLS yields to a very broad P_2 distribution between 0.2 and 1. In contrast to the R_g distributions, the P_2 distribution changes from the dimer to the trimer for each force field and shifts to lower values. By using the P_2 threshold of 0.5, AMBER, GROMOS and OPLS display 98%, 1% and 60% of disordered states for the dimer and 99%, 42% and 92% for the trimer, respectively.

The quantity $c(ij)$ probes the direction of alignment. For A β_2 , AMBER displays a flat distribution between -1 and 1. In contrast, GROMOS strongly favors antiparallel structures, the probability for $c(ij)$ between -1 and -0.75 is 96%. With OPLS we find 43% of the states with $c(ij) \leq -0.75$, 34 % with $-0.75 \leq c(ij) \leq 0$, and 23 % with $c(ij) \geq 0$.

For A β_3 , since a distribution of the $c(ij)$ of any pairs of peptides does not provide full information on the whole orientation, we calculated the conditional probability distribution $P[c(i,j)|c(i,k) \geq 0]$ ($i,j,k=1,2,3$) for finding the $c(i,j)$ between peptides i -th and j -th given the positive $c(i,k)$ between peptides i -th and k -th. The distribution $P[c(1,2)|c(1,3) \geq 0]$ is shown in Fig. 1. For each force field, the directional alignment in A β_3 is very similar to that observed in A β_2 , although the tendency to form antiparallel structures is decreased. That is, GROMOS still favors strongly antiparallel structures, while AMBER and OPLS favor weakly antiparallel structures.

Finally, Figure 1 reports the distribution of the number of inter-peptide side-chain contacts. A β_2 shows a maximum for $N_c^{\text{inter}} = 3, 10$ and 6 using AMBER, GROMOS and OPLS, respectively, while A β_3 shows a maximum are 8, 20, and 12.

In order to understand how the monomer is perturbed as the peptides assembly, we analyzed the Ramachandran plots of the five inner amino acids. Fig. 2 shows the results for A β_1 . Following the "broad" definition described in *Material and Methods*, we calculated an averaged conformational population for a state $p_s = \frac{1}{N_p N_a} \sum_{i=1}^{N_p} \sum_{j=1}^{N_a} p_i^j(s)$, where s stands for α -helix or β or coil (c) states, and N_p, N_a are the number of peptides and amino acids, respectively. We see that the Ramachandran map of each amino acid varies substantially from AMBER to GROMOS and OPLS. AMBER predicts high populations of p_α (40%) and p_{coil} (58%) while the β region is almost zero. GROMOS force field leads to a p_β of 54%, p_{coil} of 38%, and p_α of 8%. Finally, OPLS equally populates equally p_β (42%) and p_{coil} (45%)

and a little p_α (13%). We also find that GROMOS allows a small population ($\approx 3\%$) of the left-handed helix state α_L while AMBER and OPLS do not.

For the $A\beta_2$ and $A\beta_3$ systems, we calculated the averaged Ramachandran distributions $P^i(\phi, \psi) = \sum_p P^i(\phi_i^p, \psi_i^p)/p$, where ϕ_i^p, ψ_i^p pertain to the residue i -th of the p -th peptide. Fig. S1 in Supplementary Materials shows the dihedral angle probability distributions for the $A\beta_3$ system. It is striking that the distributions do not change significantly from the monomer to the trimer using AMBER. With GROMOS, p_α in the trimer is smaller ($\leq 3\%$) than that in the monomer, while p_β increases (76%), and p_{coil} decreases (21%) upon assembly. With OPLS, β and coil populations are increased and decreased (55% and 34%), respectively while the α population remains unchanged.

B. Free energy landscapes

We constructed the free energy surfaces (FES) of all systems using the dPCA method. Figure 3 shows the FES of the $A\beta_1$, $A\beta_2$ and $A\beta_3$ as a function of the first two principal components V_1 and V_2 .

Each FES exhibits several free energy minima corresponding to distinct metastable conformational states denoted as Si (i stands for the state index). To identify those states, we employ the k -means algorithm [94] as a well-established simple and fast geometric clustering method. As the number of clusters must be known beforehand in k -means, we perform a visual counting of the number of minima on each landscape, ensuring that the total population of states considered are 100 %.

The centre of each cluster shown in Figure 3 is selected as a representative of state Si and each cluster is further characterized by calculating the average values of some global and local parameters using all conformations belonging to this cluster. Results are listed in the Tables S1, S2 and S3 given in Supplementary materials for $A\beta_1$, $A\beta_2$ and $A\beta_3$, respectively.

1. $A\beta_1$ system

Five states are observed with AMBER. All of them have $N_c^{\text{intra}} = 8-10$ contacts (Table S1). The first two states S1 and S2, with populations of 52% and 16%, respectively are mainly random coil, but they differ in the conformation of Leu17. The state S3 (11 %)

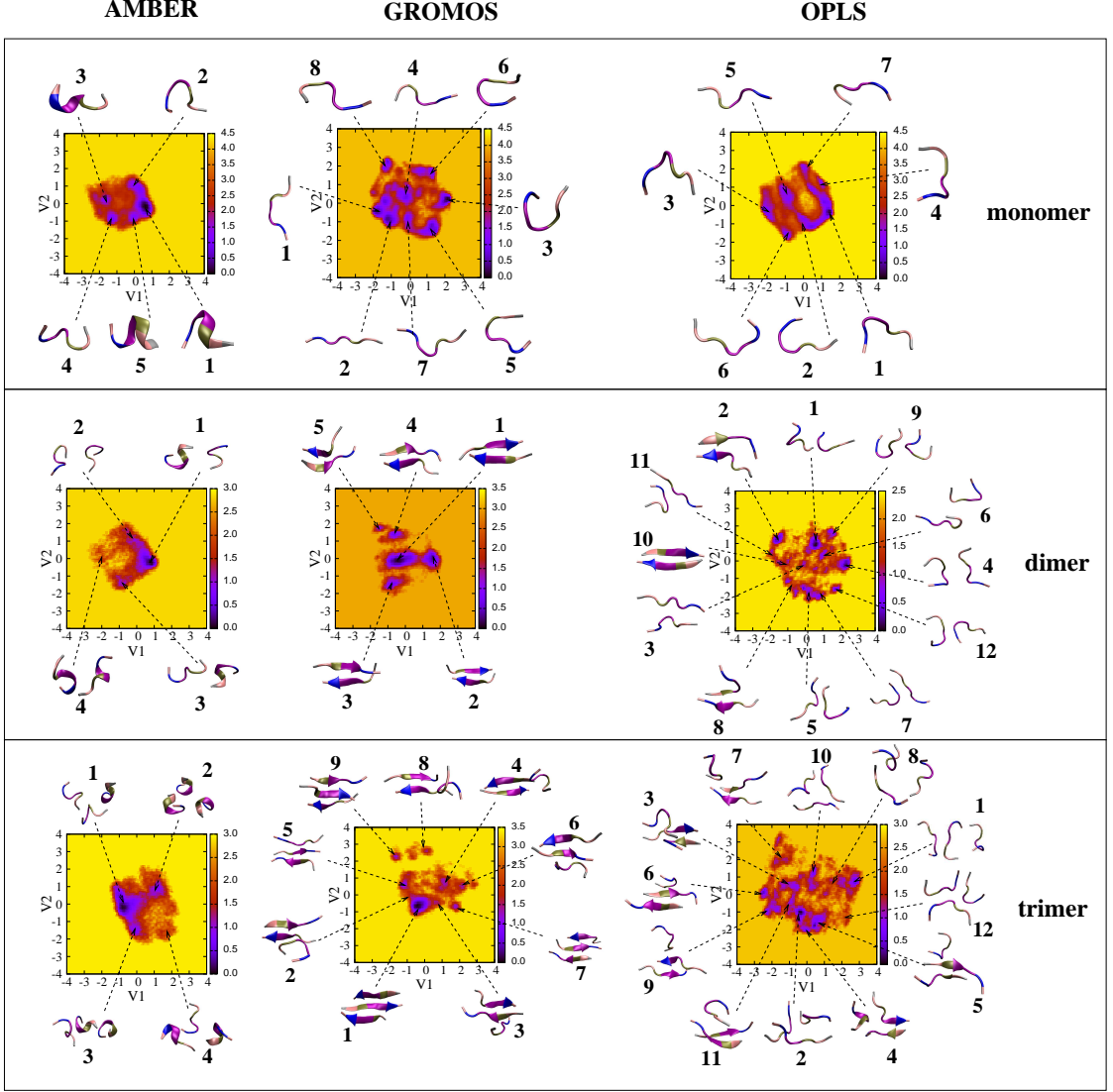


FIG. 3: Free energy landscapes (in kcal/mol) of $A\beta_1$, $A\beta_2$ and $A\beta_3$ in water as obtained from 500 ns MD simulation of $A\beta_1$ and 50 ns REMD simulations of $A\beta_2$ and $A\beta_3$, using the various force fields. Shown are results along the first two principal components obtained from the dPCA analysis. The centers of each cluster corresponding to the main minima are shown. The color gradient from black to yellow is indicative of increase in free energy.

contains both α -helix (23%) and random coil (73%) structures, and a small population (5%) of β . The last two states S4 and S5 are quite similar, i.e., both are dominated by random coil and contain small ($\approx 7\%$) populations of α -helix structure. However, their local structures differ by the conformation of Val18.

With GROMOS, we identify eight states with similar populations. The first two states

S1 and S2 are unfolded ($N_c^{\text{intra}} = 3$) and differ in the conformation of Val18. The state S3 and S6 are compact (N_c^{intra} of 10 and 8) and contain similar percentages of coil (87%). The other S4, S5, S7 and S8 are intermediates with a high percentage of coil.

With OPLS, we identify seven states with populations varying between 28 and 7%, displaying $N_c^{\text{intra}} = 4 - 6$, and essentially random coil.

2. $A\beta_2$ system

AMBER reveals four states on the free energy landscape (Fig. 3). All states are amorphous without any propensity to form fibril-like states: P_2 values of 0.3 and $c(12)$ values between the two chains varying between -0.2 and 0.1, and with a β -strand content of 0% (Table S2). They are also characterized by 8-10 intrapeptide contacts and 2-3 interpeptide contacts. In term of local structure, the dominant state S1 with a population of 53% is dominated by coil (45 %) and 3_{10} -helix (28 %). The other three states are dominated by turns and coils, and then 3_{10} -helices. Comparing the structure of peptides in the S1 of $A\beta_2$ with that of $A\beta_1$ reveals that the monomer is hardly perturbed as the peptides form dimer (RMSD between the two structures $\approx 1\text{\AA}$). This indicates that the interpeptide interactions cannot counterbalance the intrapeptide interactions.

With GROMOS, we identify five states forming only antiparallel fibril-like structures with flexibility in the extremities of the peptides and various registers of H-bonds (Fig. 3), P_2 values of 0.7-0.8 and averaged β -strand contents of 35-50% (Table S2). The structure of the monomer (Table S1) is, therefore, completely perturbed in the dimer, converting from coil to fully extended.

Using OPLS, the free energy landscape is much more complex (Fig. 3) with the presence of 12 states of similar populations (Table S2). Only two states, S2, S8 and S10 representing 24% of the total population, display partial β -sheets or full β -sheets with antiparallel arrangements. The remaining ten states are disordered ($P_2 \leq 0.5$) with high turn and coil contents and arranged in different configurations with $c(12)$ varying between -0.6 and 0.19. Compared with the $A\beta_1$ equilibrium ensemble, which displays one state with β -strand (state S3, Table S1), the peptide structure is partially perturbed upon dimerization and the conversion from coil to extended is not as significant as in GROMOS.

3. $A\beta_3$ system

As shown in Fig. 3, the free energy landscape of $A\beta_3$ obtained by AMBER exhibits four main minima. We find that the structure of each chain does not vary much from that observed in $A\beta_2$ or $A\beta_1$. As shown in Table S3, the low values of P_2 and β -strand contents, and the negative values of $c(12)$, $c(13)$ and $c(23)$ indicate that $A\beta_3$ does not form any fibril-like structures. The most populated state S1 (51 %) exhibits 28% of 3_{10} -helix and 44% of coil, whereas the less populated state S4 (7 %) still exhibits 18% of 3_{10} -helix and is dominated by turns. The other two states S2 and S3 are of coil-turn- 3_{10} -helix types.

The free energy landscape obtained by GROMOS contains nine main states with a strong preference for antiparallel β -sheet structures. The most populated state (32 %), S1, is a fully out-of-register three-stranded β -sheet, while the other states are characterized by two peptides forming an antiparallel β -sheet structure with the third peptide disordered either out-of (S4, S8) or in the plane of the β -sheet. We also find that the structures of the peptides in dimer and trimer are very similar with each others.

As expected from the dimer, the free energy landscape of $A\beta_3$ modeled by OPLS is the most complex as it exhibits many close-lying free energy minima. Nevertheless, we can identify, at least, 12 states shown in Fig. 3. All P_2 values are below the threshold value of 0.5, indicating that none of the states form a fully β -sheet structure. However, there are five states, i.e. S3, S6, S5, S7, S9, S11 displaying an antiparallel two-stranded β -sheet stabilized by a disordered peptide. We note that these structures are quite similar to the states S3, S4, S6, S7 and S8 on the free energy landscapes of $A\beta_3$ obtained by GROMOS force field. The other states, representing 54% of the total populations, are disordered with major coil and turn contents, and fewer inter-peptide contacts.

C. Temperature dependence

To determine the dependence of $A\beta_2$ and $A\beta_3$ oligomers on temperature, we calculated the three global reaction coordinates (R_g , P_2 , N_c^{inter}), the secondary structure contents and the free energy surfaces. As seen from Fig. S2 in Supplementary Materials, the three global reaction parameters depend weakly on temperature. The analysis of R_g shows that for both dimer and trimer, AMBER favors unfolded structures, whereas GROMOS and OPLS still

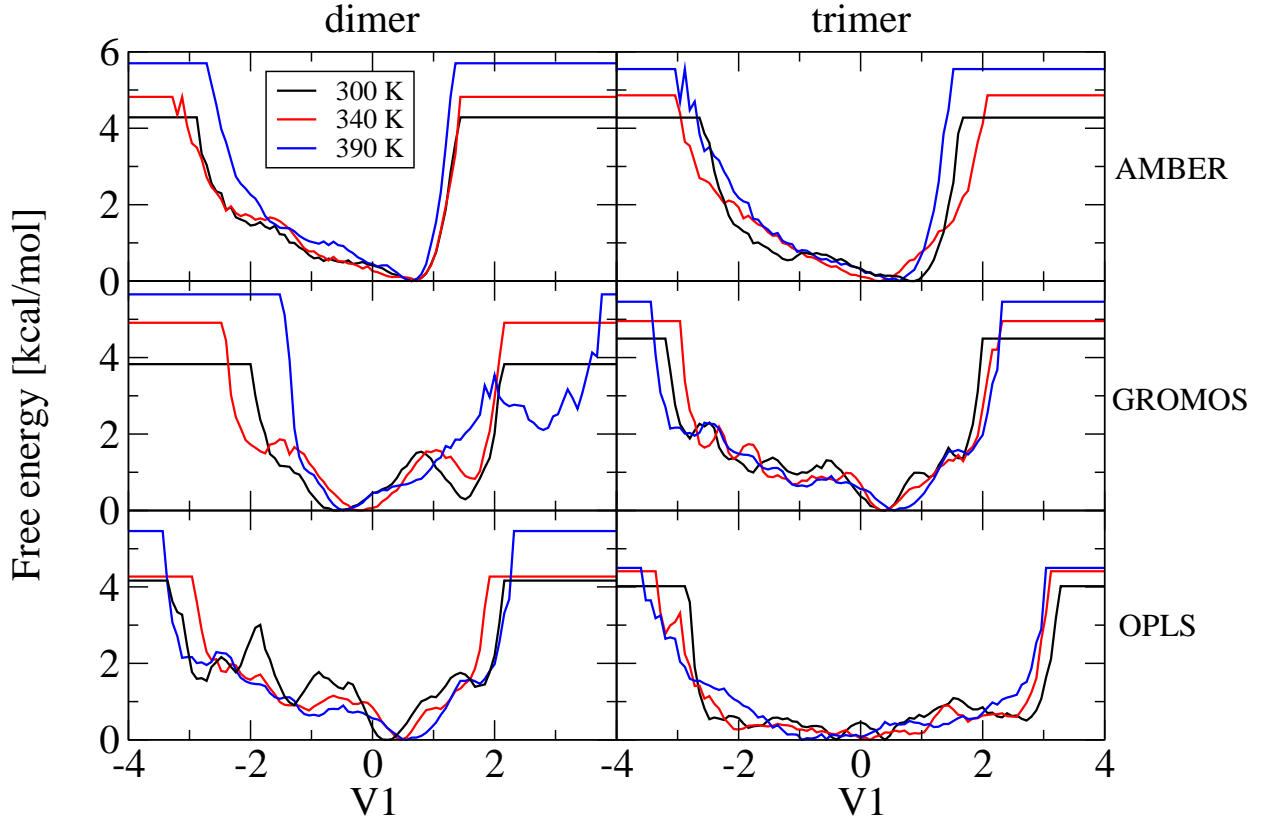


FIG. 4: Free energy landscapes of $A\beta_2$ (left panels) and $A\beta_3$ (right panels) shown as a function of the first principal component, $V1$, and three temperatures.

favor folded structures at 400 K. Both $A\beta_2$ and $A\beta_3$ oligomers are rather stable using all three force fields either in their orientations and numbers of inter-peptide contacts, P_2 and N_c^{inter} changing little as temperature is increased from 300 to 400 K.

The secondary structure contents of $A\beta_2$ and $A\beta_3$ at 300 and 400 K are compared in Table S4 given in Supplementary Materials. The small contents of α -helix, π -helix and β -bridge are not shown here. With AMBER, the 3_{10} -helix, turn and coil remain dominant at both temperatures and not change much upon heating. With GROMOS, the percentage of coil increases to 55% (dimer) and 58% (trimer), but the percentage of extended conformations remains significant at 400 K, 32% (dimer) and 17% (trimer). With OPLS, at 400 K and in both systems, the β -strand becomes marginal, and the $A\beta_2$ and $A\beta_3$ configurations are turn-coil. Interestingly, as the temperature is increased, the coil content in GROMOS is

increased while it is decreased in OPLS.

Finally, we examined how the FESs of $A\beta_2$ and $A\beta_3$ change as a function of the temperature. Here for the sake of conciseness, Fig. 4 shows the free energy along the first principal component V1, calculated for both systems and three temperatures. With AMBER, the V1 component of both systems mainly describes the fluctuation of ψ_{Val18} and ψ_{Phe19} , and the FES of each system exhibit one well-defined minimum at all temperatures. With GROMOS, the V1 of $A\beta_2$ mainly describes the fluctuation of ϕ_{Leu17} at 300 K, and also includes changes of the ψ_{Val18} and ψ_{Phe19} at 400 K. Large fluctuations of ψ_{Leu17} and ψ_{Val18} are noted in the V1 of $A\beta_3$ at both 300 K and 400 K. As seen in Fig. 4, the free energy profile at 400 K is still very similar to that at 300 K for each system. Finally, using OPLS, the V1 of $A\beta_2$ is associated with large fluctuations of ϕ_{Leu17} , ψ_{Phe19} and ψ_{Phe20} at both 300 K and 400 K. For $A\beta_3$, V1 is mainly characterized by fluctuations of ϕ_{Leu17} , ψ_{Phe19} , ψ_{Phe20} and ϕ_{Phe20} . In contrast to AMBER and GROMOS, the FES of $A\beta_3$ with OPLS is more impacted by temperature variation.

Overall our simulations indicate that increasing the temperature to 400 K impacts the dimeric and trimeric structures of $A\beta_{16-22}$ very marginally with AMBER and GROMOS and only modestly with OPLS. This is in line with the recent computational study of Best et al., which showed using AMBER ff03*, that the folded structures of the predominantly α (Trp-cage) or β (GB1 hairpin) peptides are correctly predicted at low temperatures, but the temperature dependence of their folded populations is too weak relative to experiment [72]. Looking at the helix-coil transition of polypeptides, Best et al. also found a weak temperature dependence that may result from a lack of orientational specificity in hydrogen bonding of the force field [71].

IV. DISCUSSION AND CONCLUSIONS

As the aim of this work is to study the effects of force fields on the structures of $A\beta_{16-22}$ monomer, dimer and trimer, it is important to make sure our analysis is not affected by limited sampling. Convergence of the simulations was assessed by comparing the time-averaged properties of four order parameters using block analysis, i.e. 0-25, 25-50 and 0-50 ns. Fig. 5 shows, for $A\beta_2$ and $A\beta_3$, the distribution of R_g , P_2 , the orientation between the chains, and the total inter-peptide contacts N_c^{inter} using AMBER. The superposition

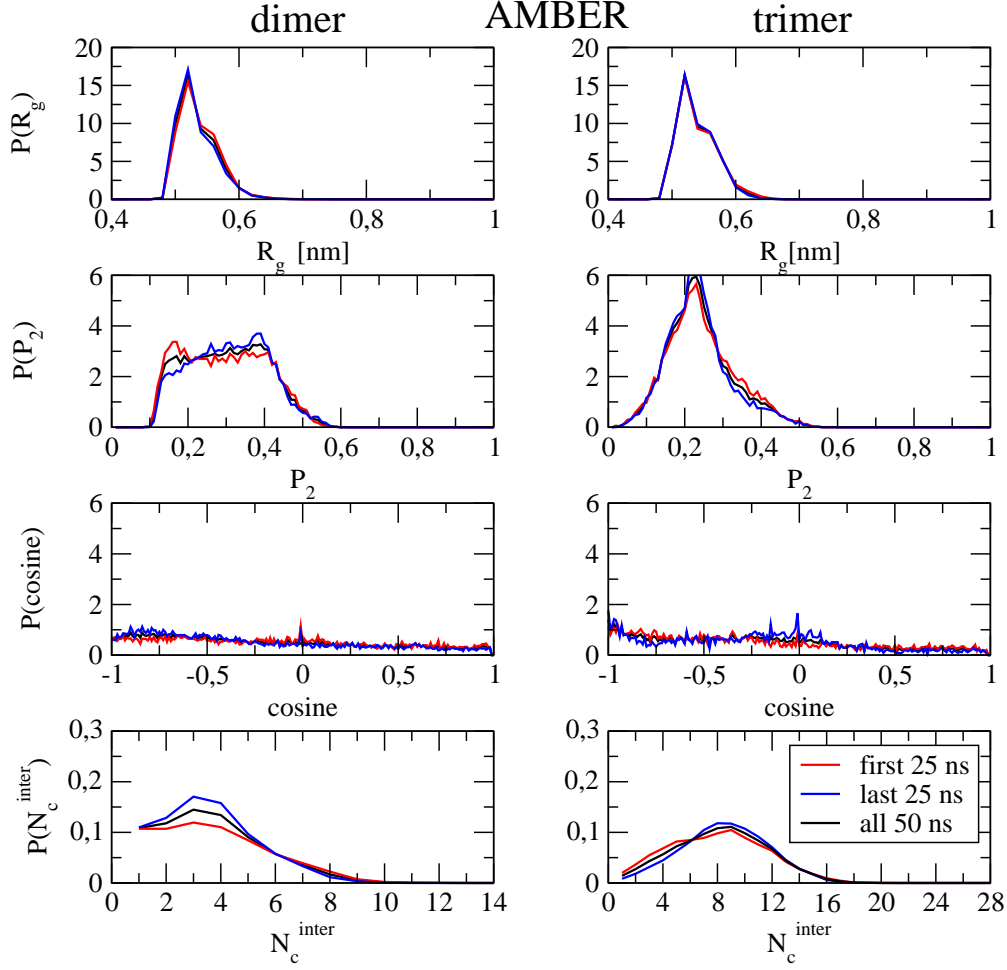


FIG. 5: Normalized distribution of the radius of gyration R_g , the order parameter P_2 , the cosine of the angle between the end-to-end vectors of two peptides referred to as $c(ij)$ for the dimer and the conditional probability for the trimer, and the total inter-peptide contacts N_c^{inter} . Shown are results obtained by the AMBER force field, using the first half (red), last half (blue) and the whole trajectory (black).

using block analysis is excellent for the four parameters. A very good convergence is also observed with GROMOS (Fig. S3 in Supplementary Materials), and only minor deviations are observed with OPLS (Fig. S4 in Supplementary materials). All together these results give us high confidence of the quality of the sampling. As our three systems have been extensively studied numerically, it is instructive to compare our results with those obtained by other force fields.

In the context of the monomer, Thirumalai and collaborators [66] reported that it adopts predominantly random coil conformations (65%) with a β -strand content of 10% based on

360 ns MD simulations using GROMOS96 and SPC model [66]. Very similar propensities were also obtained based on REMD simulations using the coarse-grained OPEP force field with implicit solvent representation [95, 96]. Similarly, Gnanakaran et al. studied the monomer of Ace-A β_{16-22} -NH₂ peptide using a modified version of the AMBER94 force field [97]. The monomer was solvated in 1583 TIP3P waters, simulated with 24 replicas between 276 and 469 K for 15 ns and the last 10 ns used for analysis. Using the generalized reaction field treatment for electrostatic interactions, they found that at 310 K the dominant monomer conformation ($\approx 40\%$) is PPII [65]. Similar results were also reported for short alanine peptides [53]. It is to be noted, however, that the difference in the β -strand and PPII populations derived from simulations and experiments is well known [46, 61, 97]. Here, we found that the coil structure is the most dominant in all three force fields with β -strand and α -helix contents varying with the force field, and the equilibrium structures are essentially compact with AMBER99, extended with GROMOS and both compact and extended with OPLS. In addition, the PPII contents of A β_1 are 0%, 14% and 2% using AMBER, GROMOS and OPLS, respectively.

In the context of the dimer, Rohrig et al. found that the antiparallel β -sheet structure is unstable by using MD, AMBER99 and TIP3P model [98]. Santini et al. used the OPEP force field and the activation-relaxation simulation technique, and found the existence of five local minima for the dimer: four antiparallel and one parallel β -sheet structures [68]. Combining OPEP with REMD, Wei et al. found six free energy minima at 310 K including in-register and out-of-register parallel strands, parallel chains, cross chains, antiparallel loops, and antiparallel strands [29]. Using the modified AMBER94 force field, Gnanakaran et al. studied the dimer solvated in a cubic box of 1626 waters using the TIP3P model and 38 replicas between 275 and 510 K for 11.5 ns and the last 6 ns used for analysis. We note that this time scale is much shorter than our time (50 ns/replica). They identified six distinct conformations for A β_2 at 310 K, including shifted parallel strand and parallel loop, parallel strand, antiparallel strand, shifted antiparallel strand, cross and tight cross/lock as shown in Fig. 1 of Ref.[65].

In this work, we found that none of the six OPEP-generated [29] or modified AMBER94-generated [65] structures of the dimer are reproduced by AMBER99, which strongly favor coil and 3_{10} -helix, and GROMOS only reproduces the antiparallel strands. In contrast, OPLS captures six structures which are similar to OPEP and modified-AMBER94 force field

calculations: S12 (shifted parallel strand), S4 (parallel strand), S10 (antiparallel strand), S3 (shifted antiparallel strand), S7 (cross) and S11 (tight cross/lock). In addition to these six minima, OPLS also identified six additional states, certainly due to the use of the dPCA analysis here vs. two simple order parameters in previous simulations [29, 65].

In the context of the trimer, Santini et al. studied the assembly using OPEP force field and the activation-relaxation simulation technique [68]. They carried out 21 simulations starting from different initial conditions, and they identified three in-register antiparallel β -sheet structures, four out-of-register antiparallel structures and one mixed parallel/antiparallel β -sheet. Favrin et al., based on an all-atom model, a home made implicit solvent representation and Monte Carlo simulations, found the predominance of mixed parallel/antiparallel β -sheets over in-register and out-of-register antiparallel β -sheets at low temperature [36]. In a recent study, Nguyen et al. reported that, these structures are essentially captured by extensive simulations using 1.3 μ s MD with GROMOS96 force field [66].

In this work, we found that none of the structures generated by OPEP are reproduced by AMBER99, which again does not form any fibril-like structures and favor strongly coil and 3_{10} -helix. The GROMOS force field coupled to REMD captures structures similar to those generated by OPEP [68] or GROMOS with long MD [66]. These structures are S1 and S7 (in-register antiparallel strand), S2, S3, S4, S5, S6 and S8 (out-of-register antiparallel strand) and S9 (mixed parallel and antiparallel) (see Fig.3, lower panel). In contrast, the OPLS force field captures out-of-register antiparallel structures (states S3, S4, S5, S6, S7, S9, S11 as seen in Fig.3, lower panel) and five disordered structures with major coil and turn contents. It does not capture, however, any in-register antiparallel or mixed parallel/antiparallel structures.

In summary, these extensive REMD simulations of the monomer to trimer of $A\beta_{16-22}$ show significant differences in the global structures, propensities of secondary structures and free energy landscapes using AMBER99, OPLS and GROMOS force fields. AMBER99 strongly favors α -helical structures in the three systems and prevents the formation of any β -sheet structures. In contrast, GROMOS favors turn-coil conformations in the monomer and a very high population of extended β -sheet structures upon assembly. In contrast, the OPLS force field shows an intermediate tendency between AMBER and GROMOS by generating diverse structures for $A\beta_1$, $A\beta_2$ and $A\beta_3$, including ordered, disordered, parallel and antiparallel structures.

There is experimental evidence that early formed oligomers are very unstable, undergoing rapid conformational transitions until the formation of a nucleus from which fibril formation is rapid, and the lag phase varies from hours to days depending on several experimental conditions. From this observation and though we cannot ignore finite size effects in our simulations, the implications of our work are as follows. Note that in principle, ab initio MD simulations of the Car-Parinello type [99, 100] or polarizable MD simulations [101] could be used to verify our results, but their applications to oligomers are not yet feasible using current computer resources. First, our all-atom simulations indicate that AMBER99 force field with TIP3P should not be used for exploring amyloid formation because of their strong biases towards α -helical structures. Second, whether the combination of GROMOS96 with the SPC water model or the combination of OPLS with the TIP3P water model is more suitable for studying the early and late steps of amyloid formation remains to be determined. But clearly both force fields should affect the aggregation kinetics and the structures of the oligomers. This has been already reported by a previous computational study on the $A\beta_{1-42}$ monomer [57]. This difference in the free energy landscapes of low molecular weight oligomers strongly suggest that the time either needed to accommodate a monomer into a fluid-like oligomer [66] and inhibit fibril growth [95, 102] may vary also substantially by using OPLS or GROMOS96.

Acknowledgments P.H.N gratefully acknowledges support from the Deutsche Forschungsgemeinschaft via a principal investigator grant (NG 87/1-1) and the Frankfurt Center for Scientific Computing. This work was also supported by the Ministry of Science and Informatics in Poland (grant No 202-204-234), the CNRS and the Institut Universitaire de France.

-
- [1] Rochet, J. C & Lansbury, P. T. (2000) *Curr. Opin. Struct. Biol.* **10**, 60–68.
- [2] Selkoe, D. J. (2003) *Nature* **426**, 900–904.
- [3] Dobson, C. M. (2004) *Science* **304**, 1259–1262.
- [4] Ross, C. A & Poirier, M. A. (2004) *Nature Med.* **10**, S10–S17.
- [5] Bossy-Wetzel, E, Schwarzenbacher, R, & Lipton, S. A. (2004) *Nature Med.* **10**, S2–S9.
- [6] Serpell, L. C, Sunde, M, Benson, M. D, Tennent, G. A, Pepys, M. B, & Fraser, P. E. (2000) *J. Mol. Biol* **300**, 1033–1039.
- [7] Sunde, M & Blake, C. (1997) *Adv. Protein Chem.* **50**, 123–159.
- [8] Harper, D. J, Lieber, C. M, & Lansbury, P. T. J. (1997) *Chem. Biol.* **4**, 951–959.
- [9] Petkova, A. T, Ishii, Y, Balbach, J. J, Antzutkin, O. N, Leapman, R. D, Delaglio, F, & Tycko, R. (2002) *Proc. Natl. Acad. Sci. USA* **99**, 16742–16747.
- [10] Antzutkin, O. N, Balbach, J. J, Leapman, R. D, Rizzo, N. W, Reed, J, & Tycko, R. (2000) *Proc. Natl. Acad. Sci. USA* **97**, 13045–13050.
- [11] Luhers, T, Ritter, C, Adrian, M, Riek-Loher, D, Bohrmann, B, H, D, Schubert, D, & Riek, R. (2005) *Proc. Natl. Acad. Sci. USA* **102**, 17342–17347.
- [12] Nelson, R, Sawaya, M. R, Balbirnie, M, Madsen, A, Riek, C, Grothe, R, & Eisenberg, D. (2005) *Nature* **435**, 773–778.
- [13] Petty, S. A & Decatur, S. M. (2005) *Proc. Natl. Acad. Sci. USA* **102**, 14272–14277.
- [14] Shim, S. H, Strasfeld, D. B, Ling, Y. L, & Zanni, M. T. (2007) *Proc. Natl. Acad. Sci. USA* **104**, 14197–14202.
- [15] Chiti, F & Dobson, C. M. (2006) *Annu. Rev. Biochem.* **75**, 333–366.
- [16] Otzen, D. E, Kristensen, O, & Oliveberg, M. (2000) *Proc. Natl. Acad. Sci. USA* **97**, 9907–9912.
- [17] Gazit, E. (2002) *J. Biol. Chem.* **16**, 77–83.
- [18] Chiti, F, Calamai, M, Taddei, N, Stefani, M, Ramponi, G, & Dobson, C. M. (2002) *Proc. Natl. Acad. Sci. USA* **99**, 14619–14625.
- [19] Kallberg, Y, Gustafsson, M, Persson, B, Thyberg, J, & Johansson, J. (2001) *J. Biol. Chem.* **276**, 12945–12950.
- [20] Chiti, F, Stefani, M, Taddei, N, Ramponi, G, & Dobson, C. M. (2003) *Nature* **424**, 805–808.

- [21] West, M. W, Wang, W. X, Patterson, J, Mancias, J. D, Beasley, J. R, & Hecht, M. H. (1999) *Proc. Natl. Acad. Sci. USA* **96**, 11211–11216.
- [22] Gupta, P, Hall, C. K, & Voegler, A. C. (1998) *Protein Sci.* **7**, 2642–2652.
- [23] Harrison, P. M, Chan, H. S, Prusiner, S. B, & Cohen, F. E. (2001) *Protein Sci.* **10**, 819–835.
- [24] Dima, R. I & Thirumalai, D. (2002) *Prot. Sci.* **11**, 1036–1049.
- [25] Li, M. S, Klimov, D. K, Straub, J. E, & Thirumalai, D. (2008) *J. Chem. Phys.* **129**, 175101.
- [26] Li, M. S, Co, N. T, Reddy, G, Hu, C. K, Straub, J. E, & Thirumalai, D. (2010) *Phys. Rev. Letts* **105**, 218101.1–218101.4.
- [27] Nguyen, H. D & Hall, C. K. (2004) *Proc. Natl. Acad. Sci. USA* **101**, 16180–16185.
- [28] Pellarin, R & Caffisch, A. (2006) *J. Mol. Biol.* **360**, 882–892.
- [29] Wei, G, Mousseau, N, & Derreumaux, P. (2007) *Prion* **1**, 3–8.
- [30] Fawzi, N. L, Kohlstedt, K. L, Okabe, Y, & Head-Gordon, T. (2008) *Biophys. J* **94**, 2007–2016.
- [31] Bellesia, G & Shea, J. E. (2009) *J. Chem. Phys.* **131**, 111102–1 – 111102–4.
- [32] Urbanc, B, Cruz, L, Yun, S, Buldyrev, S. V, Bitan, G, Teplow, D. B, & Stanley, H. E. (2004) *Proc. Natl. Acad. Sci. USA* **101**, 17345–17350.
- [33] Derreumaux, P & Mousseau, N. (2007) *J. Chem. Phys.* **126**, 025101–025106.
- [34] Gsponer, J, Haberthur, U, & Caffisch, A. (2003) *Proc. Natl. Acad. Sci. USA* **100**, 5154–5159.
- [35] Klimov, D. K & Thirumalai, D. (2003) *Structure* **11**, 295–307.
- [36] Favrin, G, Irback, A, & Mohanty, S. (2004) *Biophys. J* **87**, 3657–3664.
- [37] Buchete, N. V, Tycko, R, & Hummer, G. (2005) *J. Mol. Biol* **353**, 804–821.
- [38] Huet, A & Derreumaux, P. (2006) *Biophys. J.* **91**, 3829–3840.
- [39] Takeda, T & Klimov, D. K. (2007) *J. Mol. Biol* **368**, 1202–1213.
- [40] Bellesia, G & Shea, J. E. (2009) *J. Chem. Phys.* **130**, 145103–1 – 145103–10.
- [41] Reddy, G, Straub, J. E, & Thirumalai, D. (2009) *J. Phys. Chem. B.* **113**, 1162–1172.
- [42] Melquiond, A, Dong, X, Mousseau, N, & Derreumaux, P. (2008) *Curr Alzheimer Res.* **5**, 244–250.
- [43] Chebaro, Y, Mousseau, N, & Derreumaux, P. (2009) *J. Phys. Chem. B* **113**, 7668–7675.
- [44] van Gunsteren, W, Billeter, S. R, Eising, A. A, Hünenberger, P. H, Krüger, P, Mark, A. E, Scott, W, & Tironi, I. (1996) *Biomolecular Simulation: The GROMOS96 Manual and User Guide*. (Vdf Hochschulverlag AG an der ETH, Zurich).
- [45] Kaminski, G. A, Friesner, R. A, Tirado-Rives, J, & Jorgensen, W. L. (2001) *J. Phys. Chem.*

B **105**, 6474–6487.

- [46] Jr., A. D. M, Bashford, D, Bellott, M, Dunbrack, R. L, Evanseck, J. D, Field, M. J, Fischer, S, Gao, J, Guo, H, Ha, S, Joseph-McCarthy, D, Kuchnir, L, Kuczera, K, Lau, F. T. K, Mattos, C, Michnick, S, Ngo, T, Nguyen, D. T, Prodhom, B, III, W. E. R, Roux, B, Schlenkrich, M, Smith, J. C, Stote, R, Straub, J, Watanabe, M, Wiorkiewicz-Kuczera, J, Yin, D, & Karplus, M. (1998) *J. Phys. Chem. B* **102**, 3586–3616.
- [47] Cornell, W. D, Cieplak, P, Bayly, C. I, Gould, I. R, Jr., K. M. M, Ferguson, D. M, Spellmeyer, D. C, Fox, T, Caldwell, J. W, & Kollman, P. A. (1995) *J. Am. Chem. Soc.* **117**, 5179–5197.
- [48] Wang, J, Cieplak, P, & Kollman, P. (2000) *J. Comput. Chem.* **21**, 1049–1074.
- [49] Hornak, V, Abel, R, Okur, A, Strockbine, B, Roitberg, A, & Simmerling, C. (2006) *Proteins* **3**, 712–725.
- [50] Ono, S, Nakajima, N, Higo, J, & Nakamura, H. (2000) *J. Comput. Chem.* **21**, 748–762.
- [51] Mu, Y, Kosov, D, & Stock, G. (2003) *J. Phys. Chem. B* **107**, 5064–5073.
- [52] Yoda, T, Sugita, Y, & Okamoto, Y. (2004) *Chem. Phys. Lett.* **386**, 460–467.
- [53] Gnanakaran, S & Garca, A. E. (2005) *Proteins* **59**, 773–782.
- [54] Matthes, D & de Groot, B. L. (2009) *Biophys J.* **97**, 599–608.
- [55] Sakae, Y & Okamoto, Y. (2010) *Molecular simulation* **36**, 302–310.
- [56] Sgourakis, N. G, Merced-Serrano, M, Boutsidis, C, Drineas, P, Du, Z, Wang, C, & Garcia, A. E. (2011) *J. Mol. Biol.* **405**, 570–583.
- [57] Sgourakis, N. G, Yan, Y, MacCallum, S. A, Wang, C, & Garcia, A. E. (2007) *J. Mol. Biol.* **368**, 1448–1457.
- [58] Kent, A, Jha, A. K, Fitzgerald, J, & Freed, K. F. (2008) *J. Phys. Chem. B.* **112**, 6175–6186.
- [59] Roher, A. E, Chaney, M. O, Webster, S. D, Stine, W. B, Haverkamp, L. J, Woods, A. S, Cotter, R. J, Tuohy, J. M, Krafft, G. A, Bonnell, B. S, & Emmerling, M. R. (1996) *J. Biol. Chem.* **271**, 20631–20635.
- [60] Urbanc, B, Betnel, M, Cruz, L, G, G. B, & Teplow, D. B. (2010) *J. Am. Chem. Soc.* **132**, 4266–4280.
- [61] Dong, X, Chen, W, Mousseau, N, & Derreumaux, P. (2008) *J. Chem. Phys.* **128**, 125108–1–125108–10.
- [62] Lu, Y, Wei, G. H, & Derreumaux, P. (2011) *J. Phys. Chem. B* **115**, 1282–1288.
- [63] Ma, B & Nussinov, R. (2006) *Curr. Opin. Chem. Biol.* **10**, 445–452.

- [64] Balbach, J, Ishii, J, Antzutkin, Y, Leapman, O, Rizzo, R, Dyda, N, Reed, F, & Tycko, R. (2000) *Biochemistry* **39**, 13748–13759.
- [65] Gnanakaran, S, Nussinov, R, & Garcia, A. E. (2006) *J. Am. Chem. Soc.* **128**, 2158–2159.
- [66] Nguyen, P, Li, M. S, Staub, J. E, & Thirumalai, D. (2007) *Proc. Natl. Acad. Sci. USA* **104**, 111–116.
- [67] Santini, S, Mousseau, N, & Derreumaux, P. (2004) *J. Am. Chem. Soc.* **126**, 11509–11516.
- [68] Santini, S, Wei, G, Mousseau, N, & Derreumaux, P. (2004) *Structure* **12**, 1245–1255.
- [69] Lu, Y, Derreumaux, P, Guo, Z, Mousseau, N, & Wei, G. (2009) *Proteins* **75**, 954–963.
- [70] Freddolino, P. L, Park, S, Roux, B, & Schulten, K. (2009) *Biophys J* **96**, 3772–3780.
- [71] Best, R. B & Hummer, G. (2009) *J. Phys. Chem. B* **113**, 9004–9015.
- [72] Best, R. B & Mittal, J. (2010) *J. Phys. Chem. B* **114**, 8790–8798.
- [73] Verbaro, D, Ghosh, I, Nau, W. M, & Schweitzer-Stenner, R. (2010) *J. Phys. Chem. B* **114**, 17201–17208.
- [74] Shaw, D. E, Maragakis, P, Lindorff-Larsen, K, Piana, S, Dror, R. O, Eastwood, M, Bank, J. A, Jumper, J. M, Salmon, J. K, Shan, Y, & Wriggers, W. (2010) *Science* **330**, 341–346.
- [75] Derreumaux, P, Wilson, K. J, Vergoten, G, & Peticolas, W. L. (1989) *J. Phys. Chem.* **93**, 1338–1350.
- [76] Derreumaux, P, Vergoten, G, & Lagand, P. (1990) *J. Comput Chem.* **11**, 560–568.
- [77] Berendsen, H. J. C, Postma, J, van Gunsteren, W, & Hermans, J. (1996) *Intermolecular Forces*. (Reidel, Dordrecht).
- [78] Tirado-Rives, J & Jorgensen, W. L. (1991) *Biochemistry* **30**, 3864–3871.
- [79] Lee, J. P, Stimson, R. R, Ghilardi, J. R, Mantyh, P. W, Lu, Y. A, Felix, A. M, Llanos, W, Behbin, A, Cummings, M, Crieke, M. V, W, W. T, & Maggio, J. E. (1999) *Biochemistry* **34**, 5191–5200.
- [80] Berendsen, H. J. C, Postma, J. P. M, van Gunsteren, W. F, Dinola, A, & Haak, J. R. (1984) *J. Chem. Phys.* **81**, 3684–3690.
- [81] Berendsen, H, van der Spoel, D, & van Drunen, R. (1995) *Comp. Phys. Comm.* **91**, 43–56.
- [82] Lindahl, E, Hess, B, & van der Spoel, D. (2001) *J. Mol. Mod.* **7**, 306–317.
- [83] Ryckaert, J. P, Cicotti, G, & Berendsen, H. J. C. (1977) *J. Com. Phys.* **23**, 327–341.
- [84] Darden, T, York, D, & Pedersen, L. (1993) *J. Chem. Phys.* **98**, 10089–10092.
- [85] Patriksson, A & van der Spoel, D. (2008) *Phys. Chem. Chem. Phys* **10**, 2073–2077.

- [86] <http://folding.bmc.uu.se/remd/index.php>. (2008).
- [87] Ichiye, T & Karplus, M. (2005) *Proteins* **11**, 205–217.
- [88] Kitao, A, Hirata, F, & Go, N. (1991) *Chem. Phys.* **158**, 447–472.
- [89] Garcia, A. E. (1992) *Phys. Rev. Lett.* **68**, 2696–2699.
- [90] Amadei, A, Linssen, A. B. M, & Berendsen, H. J. C. (1993) *Proteins* **17**, 412–425.
- [91] Mu, Y, Nguyen, P. H, & Stock, G. (2005) *Proteins* **58**, 45–52.
- [92] Frishman, D & Argos, P. (1995) *Proteins* **23**, 566–579.
- [93] Garcia, A. E. (2004) *Polymer* **45**, 669–676.
- [94] Hartigan, J. A & Wong, M. A. (1979) *Applied Statistics* **28**, 100.
- [95] Chebaro, Y & Derreumaux, P. (2009) *Proteins* **75**, 442–452.
- [96] Chebaro, Y, Dong, X, Laghaei, R, Derreumaux, P, & Mousseau, N. (2009) *J. Phys. Chem. B.* **113**, 267–274.
- [97] Gnanakaran, G & Garcia, A. E. (2003) *J. Phys. Chem.* **107**, 12555–12557.
- [98] Rohrig, U. F, Laio, A, Tantalo, N, Parrinello, M, & Petrozio, R. (2006) *Biophys. J* **91**, 3217–3229.
- [99] Morante, S. (2008) *Curr Alzheimer Res.* **5**, 508–524.
- [100] Gaigeot, M. P. (2008) *J. Phys. Chem. A* **112**, 13507–13517.
- [101] Wu, J. C, Piquemal, J. P, Chaudret, R, Reinhardt, P, & Ren, P. (2010) *J. Chem. Theory. Comput.* **6**, 2059–2070.
- [102] Soto, P, Griffin, M. A, & Shea, J. E. (2007) *Biophys J* **93**, 3015–3025.